Analyst

PAPER

View Article Online
View Journal

Cite this: DOI: 10.1039/c6an00023a

Integration of a guided-mode resonance filter with microposts for in-cell protein detection†

Yi-Kai Tu,[a] Meng-Zhe Tsai,[a] I-Chin Lee,[b] Hsin-Yun Hsu[b] and Cheng-Sheng Huang*[a]

Received 5th January 2016,
Accepted 29th April 2016

DOI: 10.1039/c6an00023a

www.rsc.org/analyst

We present an integrated microfluidic system consisting of a label-free biosensor of a guided-mode resonance filter (GMRF) and a microfluidic channel with a micropost filter. The GMRF was fabricated through replica molding using an ultraviolet-curable polymer and a plastic substrate. An array of microposts (a diameter and height of 26.5 and 56 μm, respectively, and a spacing between 7.5 and 9.5 μm), fabricated on a silicon substrate through photolithography, was used as the filter. A double-sided tape was used to laminate the GMRF and a microfluidic chip such that the integrated device provides two functions: filtration of the cell debris and quantification of the in-cell protein concentration. By measuring the changes in the resonant wavelength from the GMRF, the detection of β-actin in an unprocessed lysed cell sample was demonstrated; the cell debris was separated using the micropost filter to prevent false measurement.

Introduction

Micro total analysis systems or lab-on-a-chip (LOC) systems have attracted considerable attention in the last decade because of their compactness, high sensitivity, low reagent consumption, and fast response time. The main advantage of LOC systems is their ability to integrate different functional devices into the same platform to simplify the biochemical detection procedure for proteomics, genomics, drug screening, and diagnostic applications. For fabricating a fully integrated system, many studies have focused on designing and miniaturizing various functional components, such as filters,[1,2] polymerase chain reaction microchambers,[3] micropumps and microvalves,[4] and mixers.[5] Biochips with different levels of integration[6–9] have been demonstrated, but certain traditional benchtop methods are still required for some preparation steps.

For most LOC systems, fluorescence microscopy remains the dominant detection method in conventional assays. By contrast, label-free (LF) biosensors that enable detection without requiring a fluorescent molecule offer several advantages over fluorescence microscopy and have hence gained considerable attention.[10] Among the different transducing mechanisms, LF biosensors based on optical transduction are widely used because of their high sensitivity, lack of electromagnetic interference, ability of remote sensing, multiplexing and real-time monitoring, and compact design. Using monitoring measures such as wavelength, amplitude, and coupling angle, different approaches and apparatus have been demonstrated successfully.[11] Among these, LF biosensors based on surface plasmon resonance (SPR) are the most widely used and investigated and have been used for various purposes. Desktop-sized guided-mode resonance filters [GMRFs or photonic crystals (PCs)] with advanced resolution and a simple readout system have been commercialized by several companies. Although GMRF or PC LF biosensors have been integrated into microfluidic channels,[12–14] none of these included any functional components. Until recently, Jahns *et al.*[15] incorporated a filter membrane in a microfluidic system for filtering human blood such that only blood plasma was transported to the GMRF sensor chip. However, the performance of the filter membrane and the target analyte quantification were not extensively evaluated. A major application of LOC systems is for diagnostics, in which specimens, such as a blood sample or tissue biopsy, from the human body are collected, and sample preparation steps before detection are often required. For example, to detect biomarkers in blood, a filtering step to remove cells or platelets is often necessary for accurate measurement. The detection of in-cell DNA or proteins requires cell lysis, separation, and purification before measurement. At present, these steps require certain instruments and labor to perform the task.

Here, we developed a LOC system that integrates an LF biosensor based on a GMRF and a microfluidic channel with a micropost filter such that the device can perform filtration and detection simultaneously for biomarker detection from blood samples or biomolecule detection within cells.

[a]Department of Mechanical Engineering, National Chiao Tung University, 1001 Ta Hsueh Rd., Hsinchu, Taiwan 30010. E-mail: csh@nctu.edu.tw
[b]Department of Applied Chemistry, National Chiao Tung University, 1001 Ta Hsueh Rd., Hsinchu, Taiwan 30010

†Electronic supplementary information (ESI) available. See DOI: 10.1039/c6an00023a

Materials and methods

The overall design of the LOC system and the detection setup are shown in Fig. 1. The fabrication of the LOC system consists of three main steps: GMRF fabrication, microfluidic channel fabrication, and sealing with a double-sided tape. The sample was delivered into the LOC system with a syringe from one of the inlets. When the sample flowed through the filter region, cell debris was blocked and only the protein-containing solution flowed through. The analyte was captured in the antibody-immobilized GMRF biosensor, and the analyte quantity was measured using the optical setup. Finally, the sample flowed through the outlet into the waste container.

Design and fabrication of the guided-mode resonance filter

The GMRF used consisted of a high refractive index dielectric layer coated atop a low refractive index polymeric material with a surface-relief grating structure, as shown in Fig. 2. The device functions as an optical resonator as described previously.[16–19] With proper design of the device dimensions, including the grating period and depth, dielectric layer thickness, and refractive indices (RIs) of the dielectric layer and the substrate, device resonance can be adjusted for particular applications. Resonance can be observed experimentally as a narrow-band reflection or a transmission dip when illuminated normally with a broadband light source.[20,21] The wavelength of the reflection peak or the transmission dip corresponds to the resonant wavelength. The adsorption or capture of biomolecules at the GMRF surface can change the optical thickness or the local refractive index, which alters the resonant wavelength. The amount of the shift in the resonant wavelength can be correlated with the concentration of the adsorbed biomolecules.

To fabricate the GMRF, replica molding and film deposition were used. The overall design is a three-layered structure as shown in Fig. 2. In brief, a silicon (Si) master with grating patterns was generated through electron beam lithography and etching, where the grating period, grating depth, and duty cycle were 400 nm, 140 nm, and 0.5, respectively. An optical adhesive, Norland Optical Adhesive 68 (NOA68, Norland Products Inc.), was sandwiched between the Si master and a flexible sheet of polyethylene terephthalate. After NOA68 was cured by exposure to ultraviolet (UV) light, the polymer replica was separated from the Si master. A layer of TiO_2 (thickness = 140 nm, n = 2.22) was then sputtered atop NOA68 to complete the three-layered plastic GMRF. The scanning electron microscopy (SEM) image of the top view of GMRF with a grating structure with a grating period of 400 nm and a duty cycle of approximately 0.75 is presented in Fig. 2b.

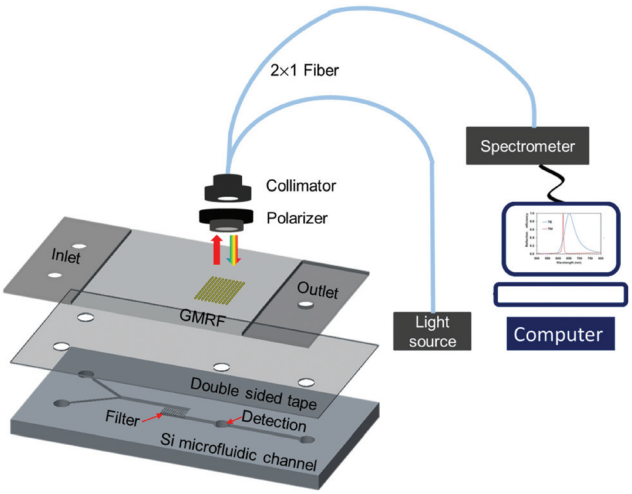

Fig. 1 Three-layered LOC system and the optical measurement setup.

Design and fabrication of the micropost filter and microfluidic channel

For clinical applications, blood serum and plasma are widely preferred because they are the most studied biological matrices for cancer biomarkers[22] and contain the whole spectrum of different biomarkers.[23] To increase sensitivity, dedicated equipment is required to remove or separate the cells and platelets from whole blood before measurement, for which a micropost array was selected because of its simplicity and effectiveness.

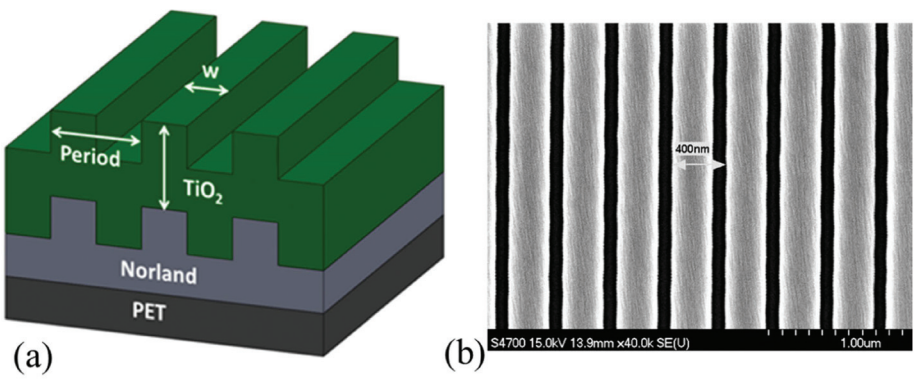

Fig. 2 (a) Schematic of a three-layered GMRF. (b) The SEM image of the top view of the GMRF with a grating period of 400 nm.

The microfluidic channel and micropost filter were fabricated simultaneously using SU-8 2035 (negative photoresist, MicroChem Corp.) through photolithography. The process began with a clean Si wafer, on which a layer of SU-8 was spin-coated. The wafer was soft-baked on a hotplate at 65 and 95 °C for 2 and 7 min, respectively. A contact aligner with a photomask was used to transfer the fluidic channel and microposts into SU-8. For post-exposure baking after UV exposure, the wafer was placed on a hotplate at 65 and 95 °C for 70 and 370 s, respectively. The film was developed in a SU-8 developer for 5 min with mild agitation, followed by rinsing with isopropyl alcohol for 1 min. Finally, to improve the structure strength and adhesion with Si, the film was hard-baked at 150 °C for 5 min. The overall SU-8 microfluidic channel is depicted in Fig. 3a.

With a reduced exposure energy (112.5 mJ cm^{-2}) relative to the manufacturer's protocol (>150 mJ cm^{-2}) and the incorporation of an I-line filter in the contact aligner, a nearly vertical (88.9°) and a high aspect ratio of microposts was obtained. As shown in Fig. 3b and c, the resulting microposts were 56.0 μm high with an extremely small T-top feature (commonly encountered in negative photoresists). The resulting top and bottom diameters of the microposts were approximately 26.5 and 23 μm, and the gap between the microposts ranged from 7.5 μm at the top to 9.5 μm at the bottom of the substrate.

Integration of the microfluidic channel, GMRF, and detection setup

The microfluidic channel and the GMRF biosensor were bonded using a double-sided tape (3M 8015P). First, the double-sided tape and GMRF sheet were drilled with holes for fluid access, which were also used for alignment to bond the top surface of the GMRF biosensor and the double-sided tape. Next, the GMRF biosensor and double-sided tape were aligned and bonded to the SU-8 microfluidic chip under a microscope. Finally, the tubing was inserted through access holes into the microfluidic channel and sealed with epoxy (8762, LETBOND). Rhodamine 6G solution was injected into the LOC system to verify the nonleaking bonding by using the proposed adhesion method (Fig. 3d–f).

A vertical experimental setup (Fig. 1) was used to measure the shift of the resonance wavelength when the sample solution flowed through the GMRF detection region. A broadband light source (LS-1-LL, Ocean Optics) connected to one end of a 2 × 1 fiber was used to illuminate the GMRF biosensor. A polarizer was placed in between the fiber and the biosensor to obtain the desired polarization. Transverse magnetic polarization was used for its narrow resonance peak, which potentially provides better resolution. The reflected light was

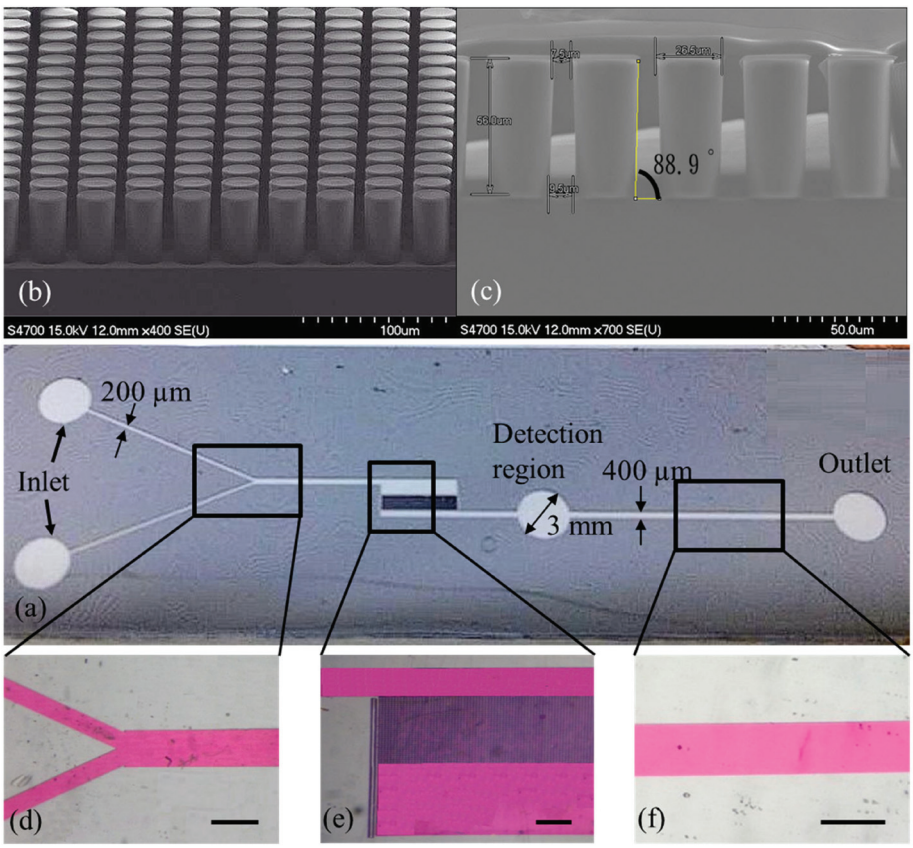

Fig. 3 (a) SEM image of the overall microfluidic chip. SEM images of (b) the tilted view of a micropost array, and (c) the cross-sectional view of microposts. (d), (e), and (f) SEM images at different sections of the microfluidic chip with a solution of Rhodamine 6G for leaking test. Scale bars = 500 μm.

collected by the same fiber and transmitted to the other end of the 2 × 1 fiber before being connected to the spectrometer (USB2000+VIS-NIR-ES, Ocean Optics) to record the spectrum.

Chip preparation for the detection of in-cell proteins

β-Actin (ACTB) is highly conserved in various organisms, including humans. However, mutations in ACTB may cause adult non-Hodgkin lymphoma. In addition, the ACTB protein is necessary in the regulation of cell motility and can modulate endothelial nitric oxide synthase, an enzyme involved in controlling the homeostasis of physiological nitric oxide production and cardiac function. Here, we demonstrated the detection of the in-cell ACTB protein from an unprocessed lysed cell solution by using the proposed LOC system. First, vapor phase deposition was used to deposit a thin layer of 3-glycidoxypropyl-trimethoxysilane on the GMRF biosensor surface for immobilizing ACTB antibodies. For this, the GMRF biosensor and 1 mL of silane solution were placed overnight in a vacuum oven at 80 °C. The biosensor was removed from the oven; sonicated in a solution of toluene, methanol, and deionized (DI) water for 2 min; and dried under a N_2 stream.

ACTB capture antibodies were diluted in 1× phosphate-buffered saline (PBS) to a concentration of 1 mg mL^{-1} and applied on the silanized GMRF surface. The biosensor was incubated for 8 h at 4 °C and 95% humidity and blocked in a solution of 1% casein (dissolved in 1× PBS) for 1 h at 4 °C. After washing in 1× PBS containing 0.05% Tween 20 (PBS-T) and DI water, the biosensor was attached to the microfluidic channel as described in the previous section. The resonant wavelength of the reflection peak measured with the biosensor filled with 1× PBS was used as the baseline signal before any measurement of the in-cell ACTB protein.

Cell harvesting and measurement

Approximately 4.5 × 10^6 cells mL^{-1} were seeded in 15 mL of Dulbecco's modified eagle medium in a 10 cm^2 dish one day before the experiment. The cells were harvested and lysed with CelLytic M cocktail [200 μL of CelLytic M (C2978, Sigma Aldrich) containing 1× protease inhibitor cocktail (Cat. G652A, Promega), and 5 μM MG132 (M7449, Sigma Aldrich)] for 30 min on ice and stored at −80 °C for later use. The total protein concentration of the cell lysate (approximately 2.55 mg mL^{-1}) was determined by using the Pierce Coomassie (Bradford) Protein Assay Kit (Thermo Fisher Scientific Inc.). For sample loading, the lysed cell samples were 10-fold diluted with 1× PBS.

Results and discussion

Bulk refractive index sensitivity measurement

For normal incidence illumination as illustrated in Fig. 1, the coupling of incident light to waveguide modes supported by a higher RI layer (TiO_2 in this work) occurs when the second-order Bragg condition is satisfied; hence, the spectral location of the transmission dip or the reflection peak can be calculated by using

$$\lambda = n_{\text{eff}}\Lambda \quad (1)$$

where λ is the resonant wavelength, n_{eff} is the effective RI, and Λ is the grating period.[24] The effective index can be regarded as the weighted average of the RIs of the GMRF.

A sucrose solution with various concentrations—0% (water only), 15%, 30%, 45%, and 60%, with the corresponding RI of 1.333, 1.356, 1.381, 1.410, and 1.442, respectively—was used to characterize the bulk RI sensitivity of the GMRF. The reflection spectra of the different solutions from one of the five experimental runs are presented in Fig. 4a (the reflection spectra of the other four runs are shown in ESI Fig. S1†). The decrease of reflection efficiency with increasing sucrose concentration indicates that the absorption of sucrose increases with the concentration. Nevertheless, the reflection peak was clear enough to be detected. By normalizing the reflection spectra from Fig. 4a, the full width at half maximum (FWHM) values decreasing with increase of sucrose concentration ranges from 5.2 to 2.9 nm for 0% to 60%. As implied by eqn (1), the resonant wavelength (or peak reflection wavelength) shifts to a longer wavelength with the increasing effective RI, which increases with the increasing RI of the solution. The peak reflection wavelength as a function of the RI is shown in Fig. 4b. The peak reflection wavelengths for each concentration from five experimental runs are summarized in Table S1 (ESI†), which indicates good consistency of the GMRF for the RI measurement. Optical biosensors based on the RI measurement are often compared for their RI sensitivity, which is defined as the ratio of the change in the resonant wavelength

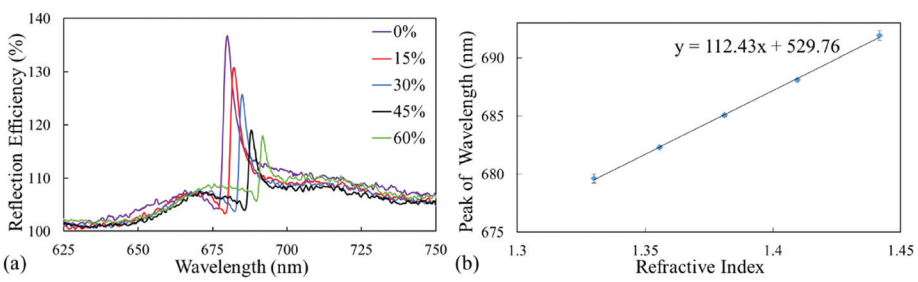

Fig. 4 (a) Reflection spectra of sucrose solutions measured at five different concentrations. (b) Peak wavelength as a function of refractive index and the linearly fitted line.

to that in the RI. The sensitivity of the designed GMRF biosensor is calculated as the slope of the linear fitted line: 112.4 nm RIU^{-1}.

In-cell protein detection

Sample solutions were loaded into the LOC system manually with a syringe. When the solution containing only dilution buffer (1× PBS, negative control) was injected into the LOC system, the peak wavelength of the reflection spectrum was used as the baseline signal. The buffer solution was subsequently extracted out before injecting the unprocessed lysed cell solution. The cell solution was incubated in the LOC system for 2 h at room temperature. The system was rinsed twice by injecting PBS-T to remove unbound analytes. PBS was again injected into the system before measuring the reflection spectrum. The same processes were repeated for other concentrations. The original reflection spectra of different concentrations from one of the experimental runs are shown in Fig. 5a. The FWHM of the normalized resonance peaks from Fig. 5a ranged from 4.7 to 6.4 nm.

By increasing the cell lysate concentration, more ACTB protein can be captured on the GMRF surface causing the peak wavelength to shift to a longer wavelength. The amount of the peak wavelength shift relative to the baseline peak as a function of the analyte concentration is summarized in Fig. 5a. The result indicates that although the total protein concentration was less than 25.5 ng mL^{-1}, and no shift in the resonance peak was detected. By contrast, at a protein concentration of more than 255 ng mL^{-1}, a 0.3 nm shift in the resonance peak was detected. As the concentration exceeded 25.5 mg mL^{-1}, the resonant wavelength remained unchanged, indicating the saturation of the ACTB protein binding to the capture antibodies. The resolution and detection limit were limited by the spectrometer and the GMRF biosensor used. With a higher resolution spectrometer, a smaller shift of peak wavelength can be measured, which could improve the detection limit. In addition, the GMRF can be further optimized[25] to have a higher sensitivity such that a small analyte concentration can result in a large peak wavelength shift, which could also improve the detection limit.

The reflection efficiency at the peak wavelength in Fig. 5a reduced with increasing protein concentration, and the results are summarized in Fig. 5b. Among different experiment runs, the efficiency of peak wavelength reflection demonstrated considerable variation, although the general trend was decreasing efficiency with increasing sample concentration. Unlike resonant wavelengths, which are mainly influenced by the degree of binding between the ACTB protein and the antibodies, the peak reflection efficiency is more susceptible to environmental conditions. Experimental lighting conditions should be more precisely controlled if the peak reflection efficiency is to be used as an alternative measurement modality.

Filtration by microposts

To facilitate an accurate measurement of the in-cell protein concentration, the cell debris is typically removed first. HEK-293 cells have a size between 10 and 30 μm. Here, a micropost array with a gap between 7.5 and 9.5 μm was used to separate the cell debris from the ACTB-containing soluble lysate. The optical microscopy images of the filtration area during sample loading (at different concentrations) are shown in Fig. 6. When the buffer solution was filled in the channel, the image shows no trapped cell debris (Fig. 6a). Once the sample was loaded into the LOC system, the cell debris was blocked by the microposts (Fig. 6b and c), and only the soluble lysate solution could flow through and reach the GMRF detection region. Although we have checked the microscopy images at the GMRF region before measurement to make sure there is no debris, we could not exclude the possibility that there might be some sub-micron debris, which was not visualized owing to the microscopic resolution; nonetheless, for the in-cell protein detection, we obtained consistent results for three independent runs and the dose–response curve could be established to calibrate the concentration. It indicated that our fabricated micropillar effectively prevented the majority of cell debris from reaching the detection zone. After this process, there might even be some minute tiny debris, it could be viewed as a background signal, which does not have severe influence on our sample measurement.

In addition, we performed an experiment to demonstrate how cell debris can cause false measurement. First, the GMRF

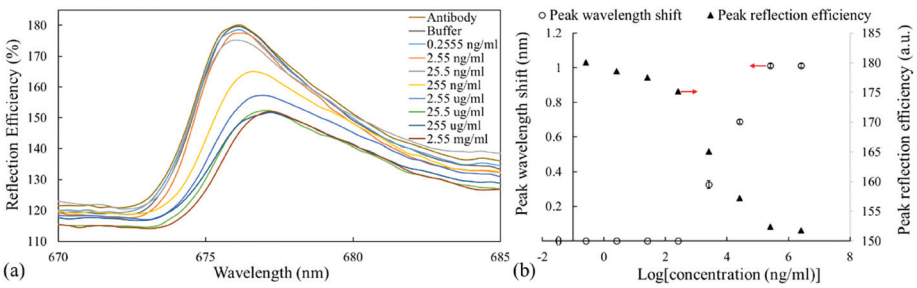

Fig. 5 (a) Original reflection spectrum when ACTB-containing protein solutions of different concentrations were injected into the LOC system. (b) The shift of the peak wavelength relative to the baseline signal as a function of ACTB protein concentration and the reflection efficiency of the peak wavelength as a function of ACTB protein concentration.

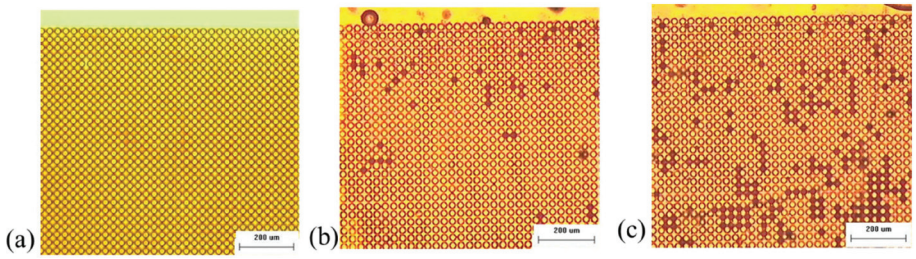

Fig. 6 Microscopy images of the micropillar regions after loading (a) control buffer solution and unprocessed cell lysates with a total protein concentration of (b) 2.55 and (c) 255 μg mL^{-1}.

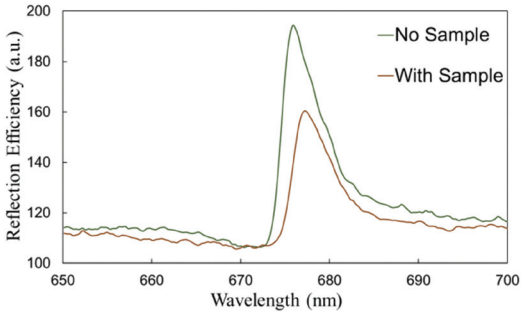

Fig. 7 Reflection spectra of the buffer solution and lysed cell sample without filtration.

biosensor was silanized and immobilized with ACTB antibodies before sealing with the microfluidic channel as described previously. The lysed cell sample (2.5 mg mL^{-1}) was injected from the outlet rather than the inlet such that both the cell debris and ACTB flowed into the GMRF detection region without passing through the filter region. The sample was then incubated for 2 h and rinsed twice with PBS-T. Finally, 1× PBS was injected into the channel before measuring the reflection spectrum. Fig. 7 shows the reflected spectrum after ACTB antibody immobilization and ACTB protein binding. The reflection peak after antibody immobilization was at 675.1 nm, and after ACTB binding, the peak wavelength shifted to 677.2 nm; that is, the peak wavelength shifted 2.1 nm. However, compared with the results shown in Fig. 5, at such a high concentration, the binding of ACTB with the antibodies reached saturation, resulting in the total peak wavelength shift of 1 nm. This result indicates that the peak wavelength shift of 1.1 nm of 2.1 nm is from the nonspecific adsorption of the cell debris on the GMRF sensor region. This implies that the microposts are necessary for separating the cell debris from reaching the detection region to prevent false detection.

Conclusions

We designed and fabricated a LOC system consisting of a microfluidic channel and a LF biosensor laminated with a double-sided tape. The microfluidic channel consists of a micropost array for filtration. A plastic GMRF was used as a LF biosensor (bulk sensitivity = 112.4 nm RIU^{-1}). When the unprocessed lysed cell sample was loaded, the integrated LOC system effectively separated the cell debris by the microposts and enabled only the soluble ACTB-containing protein solution to reach the GMRF detection region for accurate measurement. The result indicates that the fabricated LOC system can be used for ACTB detection from an unprocessed lysed sample, with a total protein concentration of 255 ng mL^{-1}.

Acknowledgements

This research was supported by the Ministry of Science and Technology (MOST), Taiwan (Grant No. NSC 101-2218-E-9-6-MY2 and MOST 103-2221-E-009-075). The authors thank the Nano Facility Center at National Chiao Tung University and National Nano Device Laboratories, Taiwan for their support in the fabrication and characterization of the GMRF and microfluidic chip.

References

1 J. Kim, M. Johnson, P. Hill and B. K. Gale, *Integr. Biol.*, 2009, **1**, 574–586.
2 S. M. Berry, E. T. Alarid and D. J. Beebe, *Lab Chip*, 2011, **11**, 1747–1753.
3 C. S. Zhang and D. Xing, *Nucleic Acids Res.*, 2007, **35**, 4223–4237.
4 C. H. Wang and G. B. Lee, *Biosens. Bioelectron.*, 2005, **21**, 419–425.
5 A. A. S. Bhagat, E. T. K. Peterson and I. Papautsky, *J. Micromech. Microeng.*, 2007, **17**, 1017–1024.
6 T. Fujii, *Microelectron. Eng.*, 2002, **61–2**, 907–914.
7 J. Khandurina, T. E. McKnight, S. C. Jacobson, L. C. Waters, R. S. Foote and J. M. Ramsey, *Anal. Chem.*, 2000, **72**, 2995–3000.
8 E. T. Lagally, P. C. Simpson and R. A. Mathies, *Sens. Actuators, B*, 2000, **63**, 138–146.
9 A. T. Woolley, D. Hadley, P. Landre, A. J. deMello, R. A. Mathies and M. A. Northrup, *Anal. Chem.*, 1996, **68**, 4081–4086.
10 X. D. Fan, I. M. White, S. I. Shopova, H. Y. Zhu, J. D. Suter and Y. Z. Sun, *Anal. Chim. Acta*, 2008, **620**, 8–26.

11 I. M. White and X. Fan, *Opt. Express*, 2008, **16**, 1020–1028.
12 C. J. Choi and B. T. Cunningham, *Lab Chip*, 2006, **6**, 1373–1380.
13 M. G. Scullion, T. F. Krauss and A. Di Falco, *Sensors*, 2013, **13**, 3675–3710.
14 G. Y. Sung, W.-J. Kim, H. Ko, B. K. Kim, K.-H. Kim, C. Huh and J. Hong, *Proc. SPIE*, 2012, **8460**, 84600F.
15 S. Jahns, P. Glorius, M. Hansen, Y. Nazirizadeh and M. Gerken, *Proc. SPIE*, 2015, **9518**, 95180K.
16 N. Ganesh, W. Zhang, P. C. Mathias, E. Chow, J. A. N. T. Soares, V. Malyarchuk, A. D. Smith and B. T. Cunningham, *Nat. Nanotechnol.*, 2007, **2**, 515–520.
17 P. C. Mathias, N. Ganesh, W. Zhang and B. T. Cunningham, *J. Appl. Phys.*, 2008, **103**, 094320.
18 D. Rosenblatt, A. Sharon and A. A. Friesem, *IEEE J. Quantum Electron.*, 1997, **33**, 2038–2059.
19 R. Magnusson and S. S. Wang, *Appl. Phys. Lett.*, 1992, **61**, 1022–1024.
20 C. S. Huang, S. George, M. Lu, V. Chaudhery, R. M. Tan, R. C. Zangar and B. T. Cunningham, *Anal. Chem.*, 2011, **83**, 1425–1430.
21 J. Ju, Y. A. Han and S. M. Kim, *Sensors*, 2013, **13**, 3232–3241.
22 S. M. Hanash, S. J. Pitteri and V. M. Faca, *Nature*, 2008, **452**, 571–579.
23 D. M. Good, V. Thongboonkerd, J. Novak, J.-L. Bascands, J. P. Schanstra, J. J. Coon, A. Dominiczak and H. Mischak, *J. Proteome Res.*, 2007, **6**, 4549–4555.
24 R. Magnusson, Y. Ding, K. J. Lee, D. Shin, P. S. Priambodo, P. P. Young and T. A. Maldonado, *Proc. SPIE*, 2003, **5225**, 20–34.
25 J. Ju, Y.-A. Han and S.-M. Kim, *Sensors*, 2013, **13**, 3232–3241.